The Inter-Layer Dependence of G-Modes in Semiconducting Double-Walled Carbon Nanotubes

D.I. Levshov,[†,‡] T. Michel,[*,†] R. Arenal,[¶,§] H. N. Tran,[†] T. X. Than,[†,‖] M. Paillet,[†] Yu. I. Yuzyuk,[‡] and J.-L. Sauvajol[†]

Laboratoire Charles Coulomb UMR 5221, Université de Montpellier - CNRS F-34095 Montpellier, France, Faculty of Physics, Southern Federal University, Rostov-on-Don, Russia, Laboratorio de Microscopias Avanzadas, Instituto de Nanociencia de Aragón, Universidad de Zaragoza, 50018 Zaragoza, Spain, ARAID Foundation, 50018 Zaragoza, Spain, and Laboratory of Carbon Nanomaterials, Institute of Materials Science, VAST, Hanoi, Vietnam

E-mail: thierry.michel@um2.fr

Phone: +33 (0)467 14 35 90. Fax: +33 (0)467 14 46 37

Abstract

A double-walled carbon nanotube (DWNT), a coaxial composite of two single-walled carbon nanotubes (SWNT), provide a unique model to study interactions between the two constituent SWNTs. Combining high resolution transmission electron

[*]To whom correspondence should be addressed
[†]Laboratoire Charles Coulomb UMR 5221, Université de Montpellier - CNRS F-34095 Montpellier, France
[‡]Faculty of Physics, Southern Federal University, Rostov-on-Don, Russia
[¶]Laboratorio de Microscopias Avanzadas, Instituto de Nanociencia de Aragón, Universidad de Zaragoza, 50018 Zaragoza, Spain
[§]ARAID Foundation, 50018 Zaragoza, Spain
[‖]Laboratory of Carbon Nanomaterials, Institute of Materials Science, VAST, Hanoi, Vietnam

microscopy (HRTEM), electron diffraction (ED) and resonant Raman scattering (RRS) experiments on the same individual suspended DWNT is the ultimate way to relate unambiguously its atomic structure, defined by the chiral indices of the coaxial outer/inner SWNTs, and its Raman-active vibration modes. This approach is used to investigate the inter-tube distance dependence of the G-modes of individual index-identified DWNTs composed of two semiconducting SWNTs. We state the main features of the dependence of the G-mode frequencies on the distance between the inner and outer layers: (i) when the inter-layer distance is larger than the nominal van der Waals distance (close to 0.34 nm), a downshift of the inner-layer G-modes in respect to the G-modes in the equivalent SWNTs is measured. (ii) the amplitude of the downshift depends on the inter-layer distance, or in other words, on the negative pressure felt by the inner layer in DWNT. (iii) no shift is observed for an inter tube distance close to 0.34 nm.

Introduction

The combination of high resolution transmission electron microscopy (HRTEM), electron diffraction (ED) and resonant Raman spectroscopy (RRS) on the same individual, spatially isolated, and suspended (environmental-free) single-walled carbon nanotube (SWNT) is the best approach to relate unambiguously structural parameters and features of Raman-active phonon modes. Up to now, only a few groups have followed this approach to determine the intrinsic features of the main Raman-active modes, namely the radial breathing mode (RBM) and the G-modes, of individual achiral and chiral, semiconducting and metallic SWNTs.[1–5] On the other hand, Raman (resonance profile), spatial modulation spectroscopy (absorption) and Rayleigh spectroscopies allow the determination of the transition energies of index-identified SWNTs.[6–10] Recently, the same approach was applied to double-walled carbon nanotubes (DWNTs).[11,12,14] A DWNT consists of two concentric and weakly van der Waals coupled SWNTs (from now, also called 'layer') and is uniquely characterized by the chiral indices (n_i, m_i) and (n_o, m_o) of the inner and outer SWNTs respectively $[(n_i, m_i)@(n_o, m_o)]$. Consequently, all the properties of DWNTs are related to the individual nature of each layer and their interactions.

Up to now, most of the Raman investigations on DWNTs have been performed on ensembles of bundles or on solution-based samples prepared by different ways such as catalytic chemical vapor deposition[15] or peapods-derived processes.[16] The earliest investigations were mainly devoted to the study of the RBM dependence of the inner and outer layers as a function of the (n, m) structure of the corresponding SWNTs. The low-frequency (high-frequency) RBM was assigned to the vibration of the outer (inner) layer, respectively. The assignment of each constituent SWNT was based on the comparison between the resonance excitation of the corresponding RBM and the calculated transition energies (the so-called Kataura plot[17]). It was also assumed that a SWNT-based Kataura plot was accurate enough for a qualitative identification of the (n,m) chiral indexes of the inner and outer layers of the

DWNTs.[18]

Following this method, a first important result was established, namely: the same inner layer can be contained inside different outer layers leading to various layer interaction strengths with respect to the inter-layer distance.[19–21] In other words, the inner layer RBM depends not only on the diameter, d_i, but also on the inner-outer layer distance, $\Delta d/2=(d_o - d_i)/2$ (where d_o (d_i) is the outer (inner) layer diameter). These results identify a DWNT as a more complex system than just a sum of constituting SWNTs. Especially, its electronic[22,23] and vibrational properties[24,25] can differ profoundly from those of the constituent SWNTs due to to layer-layer interaction.

Theoretically, it was shown that the mechanical coupling between the inner and outer layers leads to collective vibration modes, namely the so-called in-phase and out-of-phase radial breathing-like modes (RBLM). The RBLM frequencies can be quantitatively described by a coupled oscillator model and depend both on diameter and inter-layer distance (Ref.[12,24,25] and references therein). Recently, the behavior of the RBLMs in DWNTs was revisited in investigations combining HRTEM, ED and RRS on individual, spatially isolated and suspended (environment-free) DWNTs.[11,12]

By contrast, and to the best of our knowledge, no study concerning the G-modes of individual, spatially isolated and suspended index-identified SC@SC DWNTs has been reported up to now. Only few results have been obtained on individual DWNTs deposited on a substrate.[20,21,37] In these previous investigations, the inner and outer SWNTs were index-identified indirectly via the proximity of their resonance energies to the calculated transition energies of individual SWNTs.[20,21,37] The present work focus on the intrinsic behavior of G-modes of index-identified SC@SC DWNTs as a function of the diameter and inter-layer distance. A clear softening of the G-modes of the inner layer is found unambiguously when

the inter-layer distance is larger than the nominal van der Waals distance (close to 0.34 nm). The amplitude of the shift depends on the inter-layer distance and no shift is observed for an inter tube distance close to 0.34 nm.

Experimental details

The ultra-long individual double-walled nanotubes were grown by CCVD method directly on commercial perforated silicon nitride TEM grids.[26] The resonant Raman scattering measurements were performed on a Jobin Yvon T64000 spectrometer, equipped with a liquid-nitrogen-cooled silicon CCD detector, in a wide variety of excitation wavelengths by using Ar+, Kr+, He-Ne lasers and continuous Ti:sapphire and Dye lasers. The scattered light was collected through a 100x objective (N.A. = 0.95) using a back-scattering configuration. In all the measurements, both incident and scattered light polarizations are along the nanotube axis (// // polarized Raman spectrum). In order to avoid heating effects, the laser power impinging the sample was kept below 50 μW. HRTEM images and ED patterns were recorded in a FEI Titan microscope operating at 80kV and within short acquisition times (less than 5s for ED) to reduce damage induced by electron diffraction.[27,28]

Results and discussion

Figure 1 and 2 display electron diffraction patterns and low-frequency Raman spectra for two representative individual SC@SC DWNTs (tubes 5 and 6 in Table 1). Comparison between simulated, (calculated using kinematical electron theory[27–30]), and experimental electron diffraction patterns unambiguously determine the DWNT chiral indices $(n_i, m_i)@(n_o, m_o)$ to be (13,9)@(24,7) (Fig. 1a) and (22,11)@(27,17) (Fig. 2a). Table 1 summarizes the structural information derived from electron diffraction experiments on the all six index-identified incommensurate SC@SC DWNTs investigated in this work. These DWNTs have different

inter-layer distances ranging from 0.335 nm to 0.365 nm.

The low-frequency Raman spectrum of the (13,9)@(24,7) DWNT excited at 1.715 eV (Fig. 1b), and the one of the (22,11)@(27,17) DWNT excited at 1.75 eV (Fig. 2b), show two well-defined peaks. These peaks are assigned to the collective in-phase (at low-frequency) and out-of-phase (at high-frequency) RBLMs. The expected RBM frequencies of the individual SWNTs corresponding to inner (using $\omega_{RBM} = 228/d$) and outer layers (using $\omega_{RBM} = 204/d + 27$) are indicated by arrows.[11] As expected, blue-shift of the RBLM with respect to the position of the corresponding RBM is observed.[11,12,24,25]

Recently, from the modeling of the RBLMs frequencies measured on twelve individual free-standing index-identified DWNTs, Liu *et al.*[12] have been able to evaluate the coupling force constant, k_c, between the inner and outer tubes and by following, to derive the average unit-area force constant owing to tube-tube van der Waals interaction for different inter-layer distances. The comparison of these average force constants with high-pressure graphite measurements[13] allow these authors to propose a relationship between the inter-layer distance and an internal effective pressure (see Fig. 3d of Ref.[12]). They found that for inter-layer distances larger (smaller) than 0.34 nm a negative (positive) pressure occurs between the layers. Negative (positive) pressure means that the inner-outer interaction causes a slight contraction (expansion) of the outer layer concomitant with the expansion (contraction) of the inner layer (see also Ref.[31]). The same approach applied to our measurements gives unit-area force constant for a given inter-layer distance in reasonable agreement with those of Liu's and predicts an effective pressure ranging from +0.5 to -1.8 GPa for inter-layer distance between 0.335 nm and 0.365nm (see table 1).

G-modes are the other important Raman-active modes of carbon nanotubes. The features of G-modes (lineshape, frequencies, widths, relative intensity) are known to be extremely

sensitive to doping,[32] strain[33] and environmental conditions.[34] Two G-modes dominate the spectrum in a chiral SWNT, the so-called longitudinal (LO) and transverse (TO) G-mode. In achiral zigzag (armchair) SWNTs, only the LO (TO) mode is Raman active. In metallic SWNTs, on the other hand, due to the presence of a Kohn anomaly, which is associated with a strong electron-phonon coupling, the line shape of the LO mode is broad and slightly asymmetric. By contrast, this line shape is narrow and symmetric in semiconducting SWNTs.[2] The frequency of the LO and TO modes also depends on the metallic or semiconducting character of the SWNTs. The LO mode has higher (lower) frequency than the TO mode in semiconducting (metallic) SWNTs. In the diameter range 1.3-2.4 nm, the LO (TO) frequency is close to 1591 cm^{-1} in semiconducting (metallic) SWNTs, by contrast, the TO (LO) frequency of semiconducting (metallic) SWNTs is diameter-dependent: TO (LO) varies from about 1565(1555) to 1575 cm^{-1} in semiconducting (metallic) SWNTs of the same diameter range. It must be emphasized that all this detailed information concerning G-modes can only be obtained from Raman experiments on spatially isolated individual index-identified SWNTs.[2] Indeed, for bundled SWNTs or individualized SWNTs in solution the existing diameter and chirality distributions lead to the overlapping of all the modes. However, the latest progress in the enrichment of a solution containing nanotubes of particular chiralities allows the study of the G-modes' features of SWNTs in these samples.[35,36]

As a DWNT is a more complex system than SWNT, measurements on individual index-identified DWNTs are still the most optimal way to derive precise information about the G-modes' features, and especially, to shed light on the behavior of the G-modes as a function of the inter-layer distance. Previously, few results have been obtained on individual SC@SC DWNTs deposited on a substrate. In these works, the constituent SWNTs were index-identified indirectly via the proximity of their resonance energies to the calculated transition energies.[20,21,37] In particular, the figure 5 of Ref,[20] shows a sensitivity of the G^- frequencies to the strength of the inter-wall interaction.

Figure 3 displays the excitation energy dependence of the RBLMs and G-modes measured on the (13,9)@(24,7) DWNT ($\Delta d/2$ close to 0.355 nm). The use of a wide range of excitation wavelengths allows us to separate the response of the inner and outer layers of this DWNT. As a whole, for the spectrum at 2.71 eV, both inner and outer layers are observed. In the 2.18 - 2.41 eV excitation range the intense out-of-phase RBLM (associated with the resonance of the inner layer) is detected and the intense in-phase RBLM (associated with the outer layer) is measured in the 1.68 - 1.96 eV range.

As detailed in Figure 4, three G-modes are observed in the Raman spectrum excited at 2.71 eV (458 nm) meaning that both (13,9) and (24,7) layers are in resonance with the incident radiation. By fitting each component with a Lorentzian, we obtain the following frequencies: 1560, 1584 and 1592 cm^{-1} (Fig. 2.b, middle part). At 2.41 eV (514.5 nm), only the response of the inner layer is observed. The fit gives 1560 and 1584 cm^{-1} for the TO and LO components respectively (Fig. 4, top part). On the other hand, at 1.68 eV (740 nm) we observe a dominant component at 1592 cm^{-1} and a weak line at 1581 cm^{-1} assigned to the LO and TO mode of the outer layer respectively (Fig. 4, bottom part). Using the well-established diameter dependence of the G-mode frequency of SWNTs, we determine the expected frequencies of the individual (13,9) and (24,7) SWNTs respectively: for the (13,9), TO = 1569 cm^{-1} and LO = 1591 cm^{-1}; for the (24,7), TO = 1573 cm^{-1} and LO = 1591 cm^{-1}.[2] Consequently, in the (13,9)@(24,7) DWNT, the frequencies of the G-modes of the inner layer are significantly downshifted in comparison with G-modes of the corresponding (13,9) SWNT.

The main changes in the spectra presented in figure 3 occur between 1.96 eV and 2.18 eV. In order to have a more quantitative understanding of the resonances between these discrete excitation energies, excitation profiles of the RBLMs and G-modes measured, in the 1.95-2.25 eV excitation range, on the (13,9)@(24,7) DWNT are displayed in Figure 5. We

assume that the intensity of the modes as a function of laser excitation energy (E_L) is given by:

$$I(E_L)\alpha\frac{1}{[(E_L-E_{ii})^2+\frac{\Gamma^2}{4}][(E_L-E_{ii}+E_{phonon})^2+\frac{\Gamma^2}{4}]} \quad (1)$$

Where Γ is a broadening parameter, E_{ii} and E_{phonon} are the resonance and the phonon energies, respectively.

The fit of the profiles using equation 1, with E_{ii} and Γ as free parameters, shows that the out-of-phase RBLM and the G-modes located at 1560 and 1584 cm^{-1} have the same resonance energy (E_{33}^{exp} = 2.16 eV). This finding serves us as an additional criterion for the assignment of these latest G-modes to the inner layers. The experimental E_{33}^{exp} can be compared with the predicted one from Ref.[2,8] (see also Fig. 6): for the (13,9) SWNT E_{33}^{calc} = 2.27 eV (E_{44}^{calc} = 2.82 eV). Consequently, the comparison with the experimental Kataura plot established for individual SWNTs shows a downshift of about 110 meV of the E_{33} transitions of the inner layer. According to the Kataura plot, the in-phase RBLM does not show a resonance in the 1.95-2.25 eV excitation range. The observation of the G-mode at 1592 cm^{-1} has to be assigned to the scattered resonance of the G-mode of the (24,7) outer layer. The fit of the profile of the mode at 1592 cm^{-1} with Eq. 1 provides a transition energy of 1.91 eV. For the (24,7) SWNT, the following transition energies are expected: E_{33}^{calc} = 1.80 eV, E_{44}^{calc} = 1.97 eV and E_{55}^{calc} = 2.78 eV. A small shift of the E_{44} transition of the outer layer in the (13,9)@(24,7) DWNT with respect to the predicted E_{44}^{calc} for the individual (24,7) SWNT is found. Measurements of excitation profiles for several DWNTs are needed to have a more detailed understanding of their resonance energies with respect to the calculated E_{ii} in SWNTs. This work is in progress and will be presented in a future publication.

In Figure 7, the spectra measured on four representative individual SC@SC DWNTs are displayed (from the smaller (bottom) to the larger (top) inter-layer distance). In this figure, the solid arrows indicate the frequencies of the LO and TO G-modes in the corresponding in-

dividual inner SWNTs. For the (12,8)@(16,14), the spectrum is the sum of the corresponding individual inner and outer layer responses. No significant shift of the G-modes with respect to the frequencies expected for the corresponding individual (12,8) and (16,14) SWNTs is found. By contrast, and as previously detailed in the example of the (13,9)@(24,7) DWNT, the G-modes assigned to the inner layer, in the three other DWNTs, are significantly shifted with respect to the LO and TO mode of the corresponding SWNTs and larger the inter-layer distance, larger the downshift.

Similar to RBLMs, the explanation of the shift of the G-modes is likely related to the inter-layer distance, and then to a pressure effect between the inner and the outer layer. It is well-known that the vibrational modes of carbon nanotubes significantly depend on the hydrostatic pressure. For instance, Lebedkin *et al.*[38] studied the pressure dependence of the Raman-active G-modes of HiPco nanotubes dispersed in water at different excitation wavelengths. They found that TO and LO modes of single-walled carbon nanotubes have 6.5-8 cm^{-1}/GPa dependence on the compressive stress.

In the (13,9)@(24,7) DWNT, the TO and LO modes of (13,9) layer are located at 1560 cm^{-1} and 1584 cm^{-1} respectively. For an isolated (13,9) SWNT, the frequencies of the TO and LO modes are predicted to be close to 1569 and 1591 cm^{-1}, respectively. Comparing these two sets of frequencies, a frequency shift of about 9 (7) cm^{-1} for the TO (LO) G-mode of the inner layer, respectively, is found, in reasonable agreement with the extrapolation of the Lebdekin result in the negative pressure range. Indeed, a downshift of about 8-10 cm^{-1} of the TO and LO modes of the inner layer are expected for a negative pressure around -1.2 GPa.

The spectrum of the (20,4)@(20,16) DWNT (tube 4 in table 1) gives a clear evidence of the upshift of the TO G-mode of the outer layer, concomitant to the downshift of the G-

modes of the inner layer, in the negative pressure regime. Indeed, the TO G-mode assigned to the outer layer is measured at 1579.4 cm^{-1} in the (20,4)@(20,16) DWNT (Fig. 7), and it is estimated close to 1575 cm^{-1} in the (20,16) SWNT.[26]

All these dependencies are in agreement with the concept of negative pressure. Indeed, negative pressure is related to a slight contraction of the outer layer concomitant with the expansion of the inner layer.[31] The resulting stretching of the C-C bond in the inner layer explains the downshift of the inner-layer G-modes and the slight upshift of the outer layer G-modes is due to C-C contraction. Obviously, in the positive pressure regime, an opposite behavior of the G-modes of the inner (upshifted) and outer (downshifted) layers is expected. Finally, the absence of upshift in the (12,8)@(16,14) DWNT seems to suggest either that the equilibrium inter-layer distance in DWNT could be slightly smaller than 0.34 nm or that the dependence of the G-mode under pressure in DWNT is non-symmetric and depends on the direction (positive/negative) of the pressure.

The Figure 9 summarizes the dependence of the downshift between the LO (blue symbols) and TO (red symbols) of the inner layer with the corresponding G-modes in related SWNTs as a function of the inter-layer distance (or as a function of the internal pressure). The relation between the downshift of the G-modes of the inner layer and the inter-layer distance is clearly shown: larger the inter-layer distance, larger the downshift of the LO and TO G-modes. The average internal pressure slope $d\omega/dP$ from Fig. 9 is found around 4 cm^{-1}/GPa. This value is close to the one reported for external hydrostatic pressure applied to bundled DWNTs.[41] This result might indicate the hydrostatic character of the negative pressure felt by the inner layer as expected for van der Waals interation between the concentric layers.

Conclusion

In conclusion, by combining HRTEM, ED and RRS on individual, spatially isolated and suspended DWNTs, we have been able to investigate in detail the dependence of the G-modes as a function of the structural parameters of index-identified SC@SC DWNTs. We unambiguously demonstrated the dependence of the frequencies of the G-modes on the distance between the inner and outer layers. When the inter-layer distance is larger than the nominal van der Waals distance (close to 0.34 nm), a downshift of the inner-layer G-modes with respect to the corresponding modes in equivalent SWNTs is measured, and larger the inter-layer distance, larger the downshift of the LO and TO G-modes. The behavior of the G-modes is well understood by considering the effect of an effective pressure felt by the inner and outer layers. These results emphasize the importance to study individual index-identified carbon nanotubes for a detailed understanding of all their intrinsic properties.

Acknowledgment This work has been done in the framework of the GDR-E No 2756 "Science and Application of the Nanotubes-NANO-E". The authors acknowledge financial support from ANR GAMBIT,TRAIN^2 network and French Russian PICS N^0 4818. The authors thank Vincent Jourdain for helpful discussions about the synthesis of individual carbon nanotubes. The authors acknowledge financial support from RFBR grant No 15-02-08340 and funding from the Spanish Ministerio de Economia y Competitividad (FIS2013-46159-C3-3-P). The research leading to these results has received funding from the European Union Seventh Framework Program under Grant Agreement 312483 - ESTEEM2 (Integrated Infrastructure Initiative - I3) and under Grant Agreement 604391 Graphene Flagship. The microscopy work was conducted in the Laboratorio de Microscopias Avanzadas at the Instituto de Nanociencia de Aragón, Universidad de Zaragoza (Spain).

References

(1) Meyer, J.C.; Paillet, M.; Michel, T.; Moreac, A.; Neumann, A.; Duesberg, G.S.; Roth, S.; Sauvajol, J.-L. Raman modes of index-identified freestanding single-walled carbon nanotubes. *Phys. Rev. Lett.* **2005**, *95*, 217401.

(2) Paillet, M.; Michel, T.; Meyer, J.C.; Popov, V.N.; Henrard, L.; Roth, S.; Sauvajol, J.-L. Raman active phonons of identified semiconducting single-walled carbon nanotubes. *Phys. Rev. Lett.* **2006**, *96*, 257401.

(3) Débarre, A.; Kobylko, M.; Bonnot, A.-M.; Richard, A.; Popov, V.N.; Henrard, L.; Kociak, M. Electronic and mechanical coupling of carbon nanotubes: a tunable resonant Raman study of systems with known structures. *Phys. Rev. Lett.* **2008**, *101*, 197403.

(4) Michel, T.; Paillet, M.; Nakabayashi, D.; Picher, M.; Jourdain, V.; Meyer, J.C.; Zahab, A.A.; Sauvajol, J.-L. Indexing of individual single-walled carbon nanotubes from Raman spectroscopy. *Phys. Rev. B* **2009**, *80*, 245416.

(5) Liu, K.; Wang, W.; Wu, M.; Xiao, F.; Hong, X.; Aloni, S.; Bai, X.; Wang, E.; Wang, F. Intrinsic radial breathing oscillation in suspended single-walled carbon nanotubes. *Phys. Rev. B* **2011**, *83*, 131404.

(6) Sfeir, M. Y.; Wang, F.; Huang, L.; Chuang, C. C.; Hone, J.; O'Brien, S.; Heinz, T.; Brus, L.E. Probing electronic transitions in individual carbon nanotubes by Rayleigh scattering. *Science* **2004**, *306*, 1540.

(7) Sfeir, M. Y.; Beetz, T.; Wang, F.; Huang, L.; Henry Huang, X. M.; Huang, M.; Hone, J.; O'Brien, S.; Misewich, J. A.; Heinz, T. et al. Optical spectroscopy of individual single-walled carbon nanotubes of defined chiral structure. *Science* **2006**, *312*, 554.

(8) Michel, T.; Paillet, M.; Meyer, J.C.; Popov, V.N.; Henrard, L.; Sauvajol, J-L E_{33} and E_{44} Optical transitions in semiconducting single-walled carbon nanotubes: electron diffraction and Raman experiments. *Phys. Rev. B* **2007**, *75*, 155432.

(9) Liu, K.; Deslippe, J.; Xiao, F.; Capaz, R.B.; Hing, X.; Aloni, S.; Zettl, A.; Wang, W.; Bai, X.; Louie, S. G. et al. An atlas of carbon nanotube optical transitions. *Nat. Nanotech.* **2012**, *7*, 325.

(10) Blancon, J.-C.; Paillet, M.; Tran, H. N.; Than, X. T.; Guebrou, S. A.; Ayari, A.; san Miguel, A.; Phan, N.-M.; Zahab, A. A.; Sauvajol, J.-L. et al. Direct measurement of the absolute absorption spectrum of individual semiconducting single-wall carbon nanotubes. *Nature Comm.* **2013**, *4*, 2542.

(11) Levshov,D.; Than, T. X.; Arenal, R.; Popov, V. N.; Parret, R.; Paillet, M.; Jourdain, V.; Zahab, A. A.; Michel, T.; Yuzyuk, Yu. I. et al. Experimental evidence of a mechanical coupling between layers in an individual double-walled carbon nanotube. *Nano Lett.* **2011**, *11*, 4800.

(12) Liu, K.; Hong, X.; Wu, M.; Xiao, F.; Wang, W.; Bai, X.; Ager, J. W.; Aloni, S.; Zettl, A.; Wang, E. et al. Quantum-coupled radial-breathing oscillations in double-walled carbon nanotubes. *Nat. Commun.* **2013**, *4*, 1375.

(13) Hanfland, M.; Beister, H.; Syassen, K. Graphite under pressure: Equation of state and first-order Raman modes *Phys. Rev. B* **1989**, *39*, 12598.

(14) Levshov, D.; Michel, T.; Paillet, M.; Than, X. T.; Tran, H. N.; Arenal, R.; Rahmani, A.; Boutahir, M.; Zahab, A.A.; Sauvajol, J.-L. Coupled vibrations in index-identified carbon nanotubes. *MRS Proceedings* **2014**, 1700.

(15) Endo, M.; Muramatsu, H.; Hayashi, T. A.; Kim, Y. A.; Terrones, M.; Dresselhaus, M. S. Nanotechnology: 'Buckypaper' from coaxial nanotubes. *Nature* **2005**, *433*, 476.

(16) Bandow, S.; Hiraoka, T.; Yumura, T.; Hirahara, K.; Shinohara, H.; Iijima, S. Raman scattering study on fullerene derived intermediates formed within single-wall carbon nanotube: from peapod to double-wall carbon nanotube. *Chem. Phys. Lett.* **2004**, *384*, 320.

(17) Kataura, H.; Kumazawa, Y.; Maniwa, Y.; Umezu, I.; Suzuki, S.; Ohtsuka, Y.; Achiba, Y. Optical properties of single-wall carbon nanotubes. *Synth. Met.* **1999**, *103*, 255.

(18) Villalpando-Paez, F.; Moura, L. G.; Fantini, C.; Muramatsu, H.; Hayashi, T.; Kim, Y. A.; Endo, M.; Terrones, M.; Pimenta, M. A.; Dresselhaus, M. S. Tunable Raman spectroscopy study of CVD and peapod-derived bundled and individual double-wall carbon nanotubes. *Phys. Rev. B* **2010**, *82*, 155416.

(19) Pfeiffer,R.; Simon, F.; Kuzmany, H.; Popov, V.N.; Zlyomi, V.; Krti, J. Tube-tube interaction in double-wall carbon nanotubes. *Phys. Stat. Sol. b* **2006**, *243*, 3268.

(20) Villalpando-Paez, F.; Muramatsu, H.; Kim, Y. A.; Farhat, H.; Endo, M.; Terrones, M.; Dresselhaus, M. S. Wall-to-wall stress induced in (6,5) semiconducting nanotubes by encapsulation in metallic outer tubes of different diameters: a resonance Raman study of individual C60-derived double-wall carbon nanotubes. *Nanoscale* **2010**, *2*, 406.

(21) Hirschmann, T. C.; Araujo, P. T.; Muramatsu, H.; Rodriguez-Nieva, J. F.; Seifert, M.; Nielsch, K.; Kim, Y. A.; Dresselhaus, M. S. Role of intertube interactions in double- and triple-walled carbon nanotubes. *ACS Nano* **2014**, *8*, 1330.

(22) Liu, K. ; Jin, C. ; Hong, K. ; Kim, J. ; Zettl, A.; Wang, E. ; Wang, F. Van der Waals-coupled electronic states in incommensurate double-walled carbon nanotubes *Nature Phys.* **2014** *10*, 737-742.

(23) M. Koshino, M. ; Moon, P. ; Son, Y.W. Incommensurate double-walled carbon nanotubes as one-dimensional moiré crystals *Phys. Rev. B* **2015**, *91*, 035405.

(24) Popov, V.N.; Henrard, L. Breathinglike phonon modes of multiwalled carbon nanotubes. *Phys. Rev. B* **2002**, *65*, 235415.

(25) Dobardzić, E.; Maultzsch, J.; Milosević, I.; Thomsen, C.; Damnjanović, M.E. The radial breathing mode frequency in double-walled carbon nanotubes: an analytical approximation. *Phys. Stat. Solidi B* **2003**, *237*, R7-R10.

(26) Tinh, T. X.; Nguyen, V. C.; Jourdain, V.; Paillet, M.; Kim, D.-Y.; Sauvajol, J.-L.; Ngo, T. T. T.; Phan, N. M. Synthesis of individual ultra-long carbon nanotubes and transfer to other substrates. *J. Exp. Nanosci.* **2011**, *6*, 547.

(27) Arenal, R.; Loethman, P.; Picher, M.; Than, T.; Paillet, M.; Jourdain, V. Direct evidence of atomic structure conservation along ultra-long carbon nanotubes. *J. of Phys. Chem. C* **2012**, *116*, 14103.

(28) Arenal, R.; Kociak, M.; Loiseau, A.; Miller, D.J. Determination of chiral indices of individual single- and double-walled boron nitride nanotubes by electron diffraction. *Applied Physics Letters* **2006**, *89*, 073104.

(29) Lambin, P.; Lucas, A. Quantitative theory of diffraction by carbon nanotubes. *Phys. Rev. B* **1997**, *56*, 3571.

(30) Kociak, M.; Hirahara, K.; Suenaga, K.; Iijima, S. How accurate can the determination of chiral indices of carbon nanotubes be? *Eur. Phys. J. B* **2003**, *32*, 457-469.

(31) Christofilos, D.; Arvanitidis, J.; Kourouklis, G. A.; Ves, S.; Takenobu, T.; Iwasa, Y.; Kataura, H. Identification of inner and outer shells of double-wall carbon nanotubes using high-pressure Raman spectroscopy *Phys. Rev. B* **2007**, *76*, 113402.

(32) Rao, A. M.; Eklund, P. C.; Bandow, S.; Thess, A.; Smalley, R. E. Evidence for charge transfer in doped carbon nanotube bundles from Raman scattering. *Nature* **1997**, *388*, 257-259.

(33) Levshov, D. I.; Yuzyuk, Yu. I.; Michel, T.; Voisin, C.; Alvarez, L.; Berger, S.; Roussignol, P.; Sauvajol, J.-L. Raman probing of uniaxial strain in individual single-wall carbon nanotubes in a composite material. *J. Phys. Chem. C* **2010**, *114*, 16210.

(34) Nguyen, K. T.; Gaur, A.; Shim, M. Fano lineshape and phonon softening in single isolated metallic carbon nanotubes. *Phys. Rev. Lett.* **2007**, *98*, 145504.

(35) Haroz, E. H.; Duque, J. G.; Rice, W. D.; Densmore, C. G.; Kono, J.; Doorn, S. K. Resonant Raman spectroscopy of armchair carbon nanotubes: absence of broad G^- feature. *Phys. Rev. B* **2011**, *84*, 121403.

(36) Telg, H.; Duque, J. G.; Staiger, M.; Tu, X.; Hennrich, F.; Kappes, M. M.; Zheng, M.; Maultzsch, J.; Thomsen, C.; Doorn, S. K. Chiral index dependence of the G^+ and G^- Raman modes in semiconducting carbon nanotubes. *ACS Nano* **2012**, *6*, 904.

(37) Villalpando-Paez, F.; Son, H.; Nezich, D.; Hsieh, Y. P.; Kong, J.; Kim, Y. A.; Shimamoto, D.; Muramatsu, H.; Hayashi, T.; Endo, M. et al. Raman spectroscopy study of isolated double-walled carbon nanotubes with different metallic and semiconducting configurations. *Nano Lett.* **2008**, *8*, 3879.

(38) Lebdekin, S.; Arnold, K.; Kiowski, O.; Hennrich, F.; Kappes, M. Raman study of individually dispersed single-walled carbon nanotubes under pressure. *Phys. Rev. B* **2006**, 73, 094109.

(39) Levshov, D. I.; Avramenko, M.V.; Than, T.; Michel, T.;Arenal, R;Paillet, M.; Rochal, S. B.; Yuzyuk, Yu. I.; Sauvajol, J.-L. The study of low-frequency col-

lective modes in double-walled carbon nanotubes: the continuous 2D membrane theory. *Journal of Nanoelectronics and Optoelectronics* **2015**, *10*, *in press*.

(40) Paillet, M.; Michel, T.; Zahab, A. A.; Nakabayashi, D.; Jourdain, V.; Parret, R.; Meyer, J.C.; Sauvajol, J.-L. Probing the structure of single-walled carbon nanotubes by resonant Raman scattering. *Phys. Stat. Solidi b* **2010**, *247*, 2762.

(41) Aguiar, A. L.; Barros, E. B.; Capaz, R. B.; Souza Filho, A. G.; Freire, P. T. C.; Mendes Filho, J.; Machon, D.; Caillier, Ch.; Kim, Y. A.; Muramatsu, H. et al. Pressure-induced collapse in double-walled carbon nanotubes: chemical and mechanical screening effects. *J. Phys. Chem. C* **2011**, *115*, 5378.

Table 1: The structural information derived from electron diffraction experiments on the six SC@SC DWNTs investigated in this work. The effective pressure calculated from the model presented in Ref.[12]

Label	Indices	Diameter (nm)	Chiral angles (degree)	Type $2n+m$	$\Delta d/2$ (nm)	Effective pressure (GPa)
Tube 1	(12,8)@(16,14)	1.366@2.037	23.41@27.8	2@1	0.335	0.5
Tube 2	(16,12)@(27,10)	1.905@2.595	25.28@15.14	1@2	0.345	-0.5
Tube 3	(10,9)@(18,11)	1.289@1.985	28.26@22.07	2@2	0.348	-0.8
Tube 4	(20,4)@(20,16)	1.745@2.447	8.95@26.33	2@2	0.351	-1.0
Tube 5	(13,9)@(24,7)	1.501@2.206	24.01@12.43	2@1	0.353	-1.1
Tube 6	(22,11)@(27,17)	2.280@3.011	19.11@22.52	1@2	0.365	-1.8

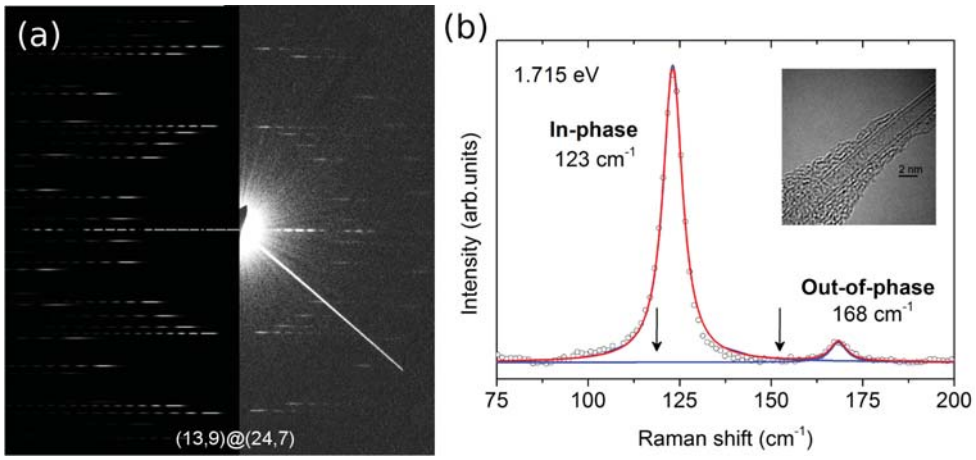

Figure 1: (a) Comparison of the simulated (left) and experimental (right) electron diffraction patterns of the (13,9)@(24,7) DWNT. (b) The low-frequency range of the Raman spectrum of the (13,9)@(24,7) DWNT excited at 1.715 eV. The arrows indicate the frequencies of the RBM of related individual outer and inner SWNTs. The spectra are fitted with Lorentzian. Insert: HRTEM micrograph of the DWNT. Amorphous carbon was deposited during TEM analysis.

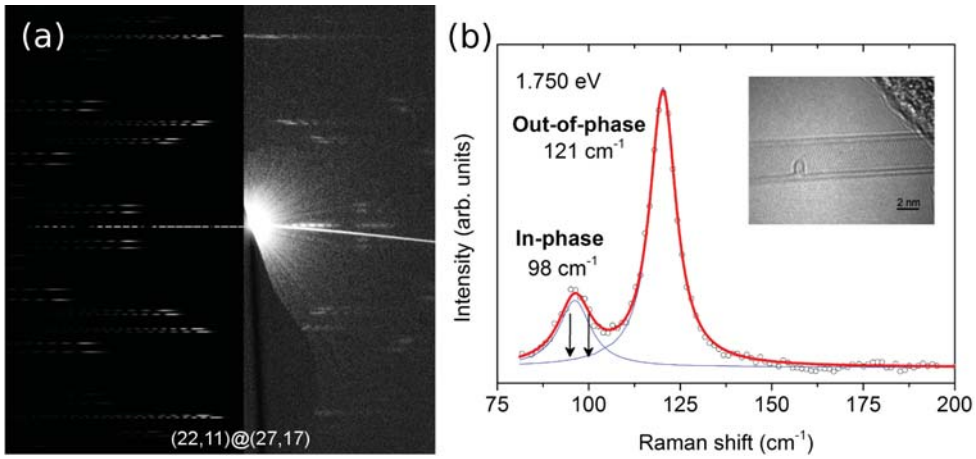

Figure 2: (a) Comparison of the simulated (left) and experimental (right) electron diffraction patterns of the (22,11)@(27,17) DWNT. (b) The low-frequency range of the Raman spectrum of the (22,11)@(27,17) DWNT excited at 1.750 eV. The arrows indicate the frequencies of the RBM of related individual outer and inner SWNTs. The spectra are fitted with Lorentzian. Insert: HRTEM micrograph of the DWNT.

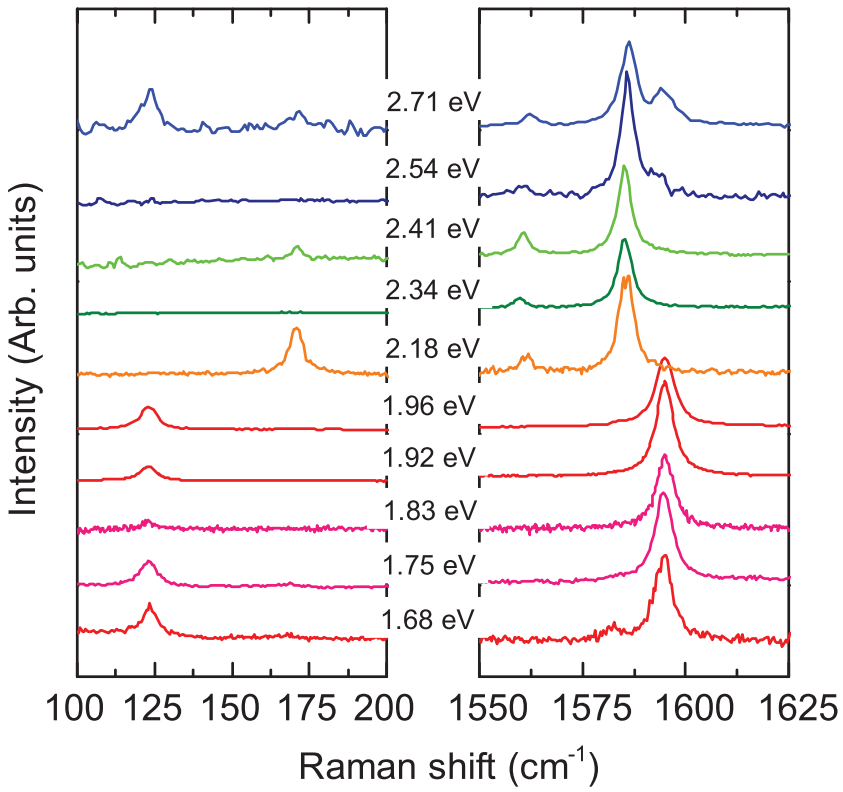

Figure 3: RBLM and G-modes range of the Raman spectrum of the (13,9)@(24,7) DWNT excited at different energies indicated in the figure. The spectra are normalized for clarity.

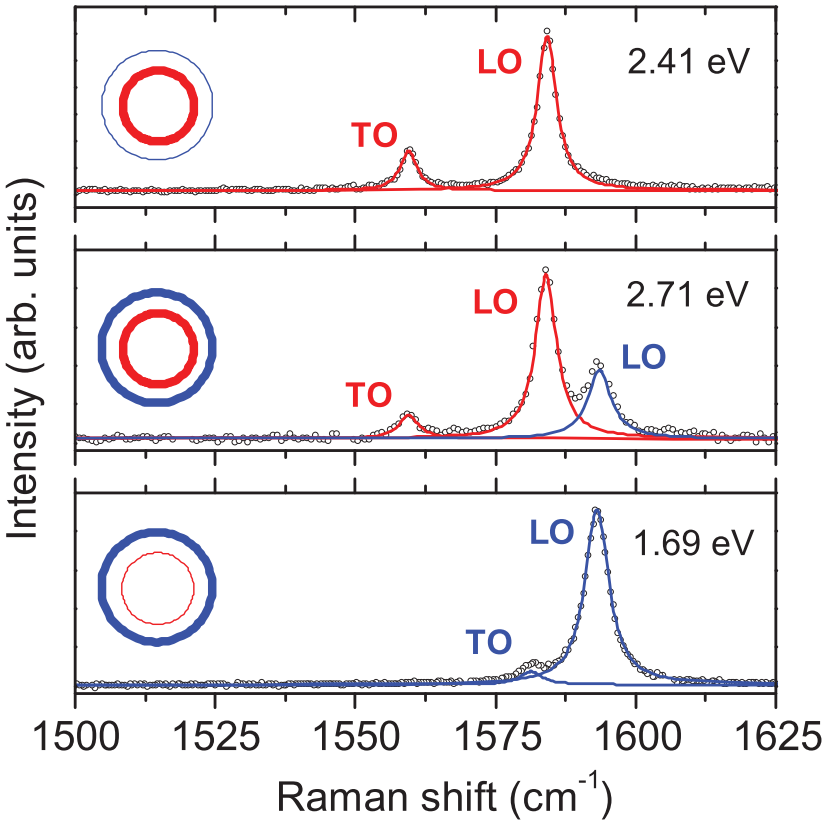

Figure 4: Details of the excitation dependence of the G-modes range of the Raman spectrum of the (13,9)@(24,7) DWNT, (from top to bottom: 2.41, 2.71, 1.69 eV). Inset: A sketch of the DWNT for each excitation energy, bold contour means that the corresponding SWNT is in resonance and a thin contour means that the corresponding SWNT is off resonance.

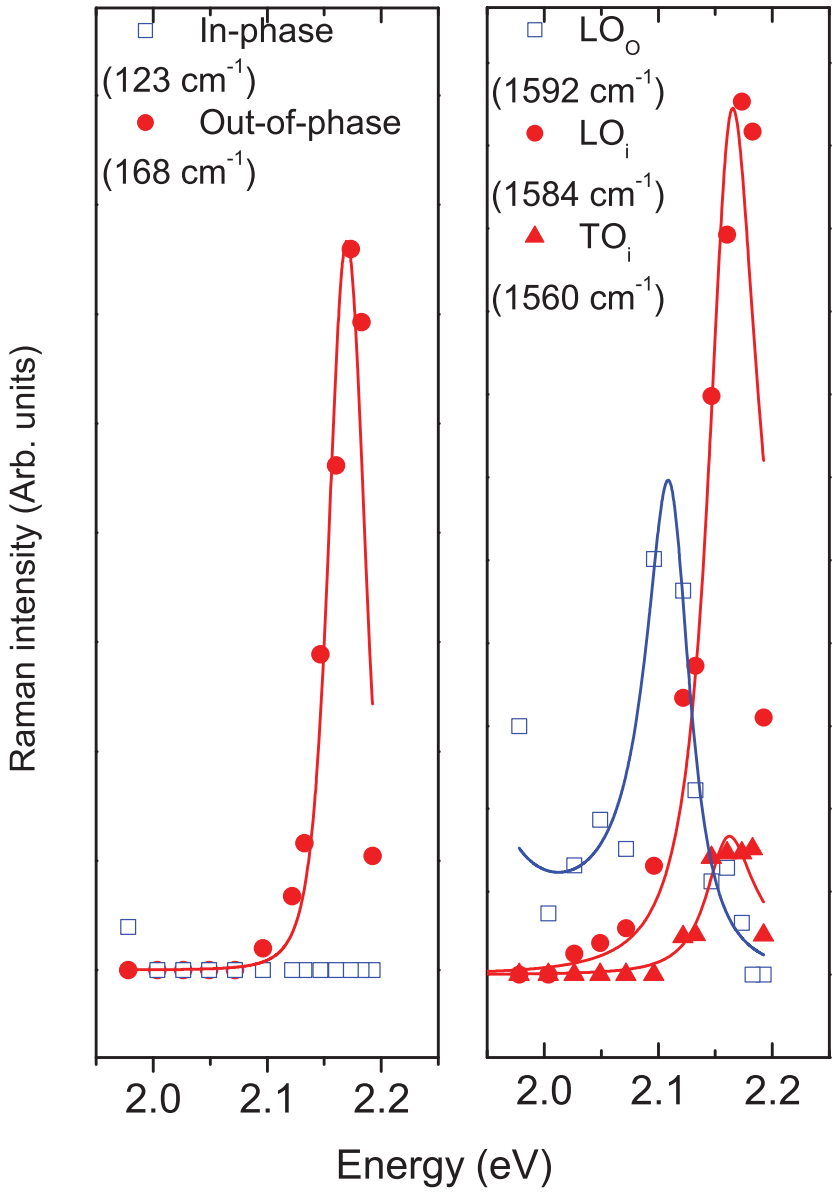

Figure 5: Excitation profiles of the RBLMs and G-modes of the (13,9)@(24,7) DWNT measured in the 1.95-2.25 eV excitation range.

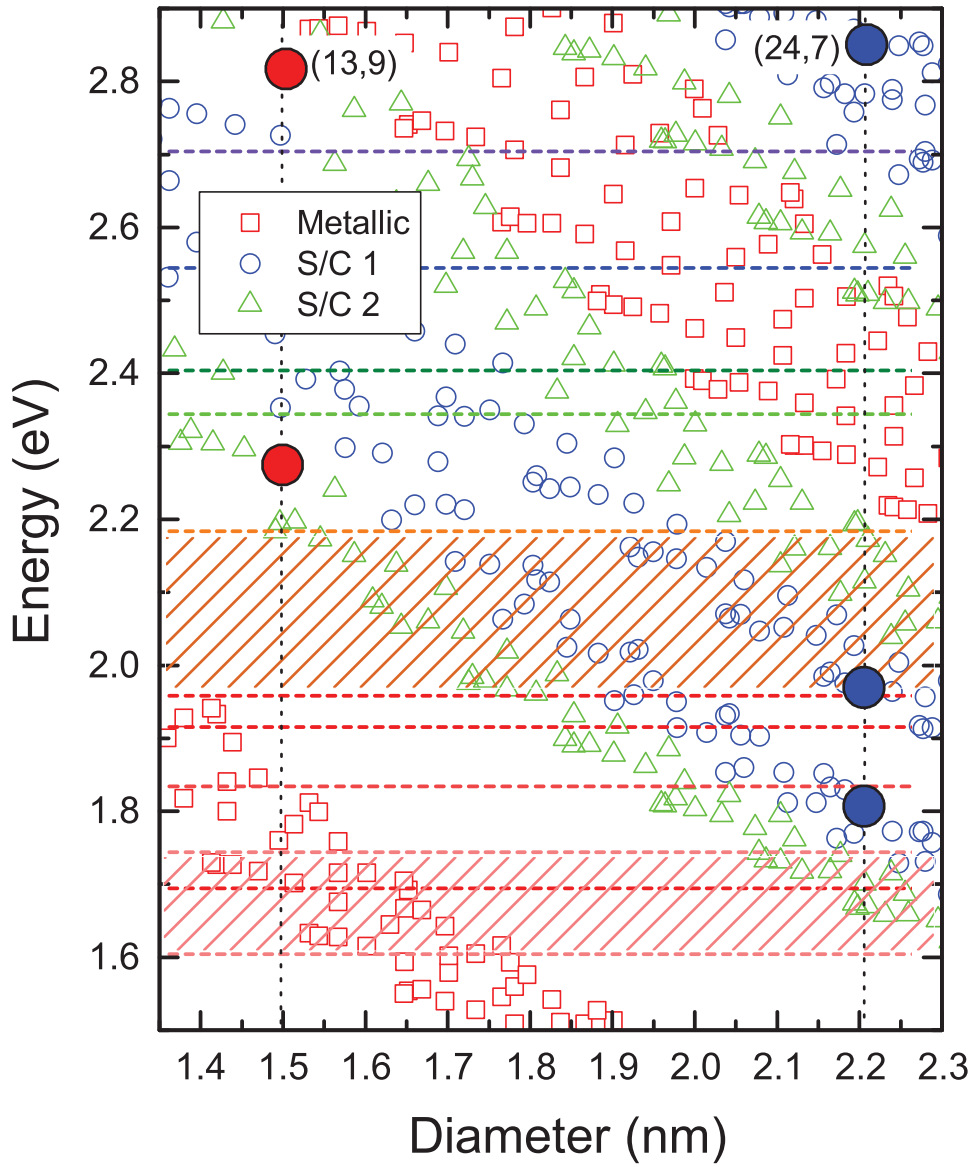

Figure 6: Part of the Kataura plot (from Ref.[8]) related to the resonance energy range of the (13,9)@(24,7) DWNT. The solid dots indicate the transition energies expected for the individual inner SWNT (red) and outer SWNT (blue) respectively. The horizontal dotted lines mark the excitation energies where Raman spectra were acquired. The hatched areas indicate regions where Raman spectra were acquired in $\approx$ 25 meV intervals.

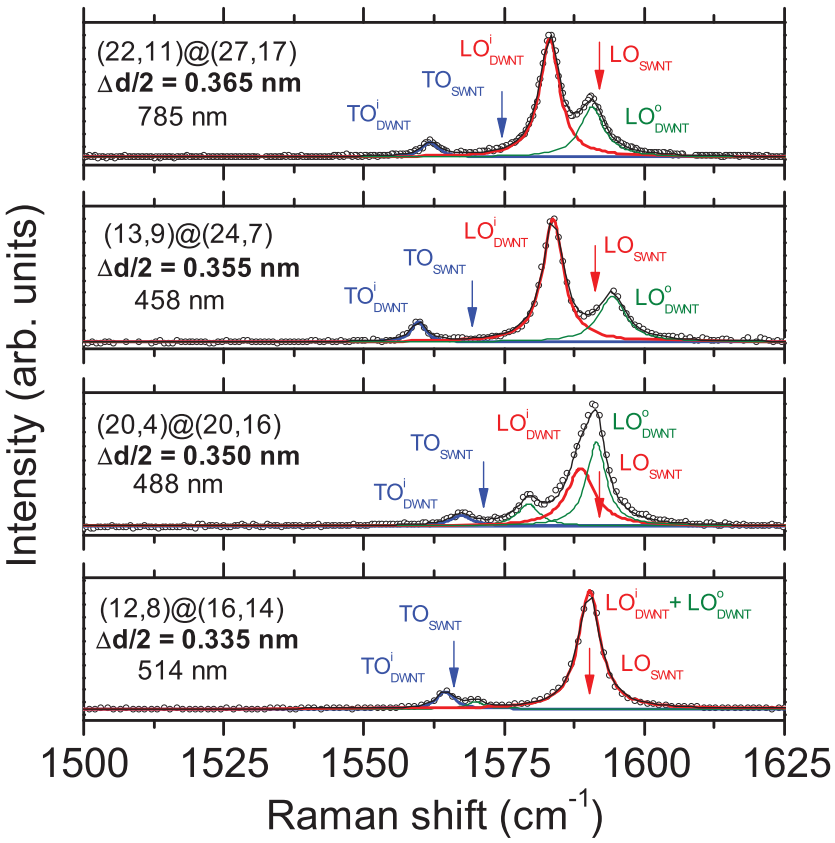

Figure 7: Comparison of the G-modes measured on four SC@SC DWNTs (from top to bottom (12,8)@(16,14), (20,4)@(20,16), (13,9)@(24,7), (22,11)@(27,17)). The inter-layer distance increases from bottom to top (0.335, 0.350, 0.355, 0.365 nm). Arrows mark the expected frequencies of the LO mode (red) and TO mode (blue) in the corresponding individual inner SWNTs. The spectra are fitted with Lorentzians.

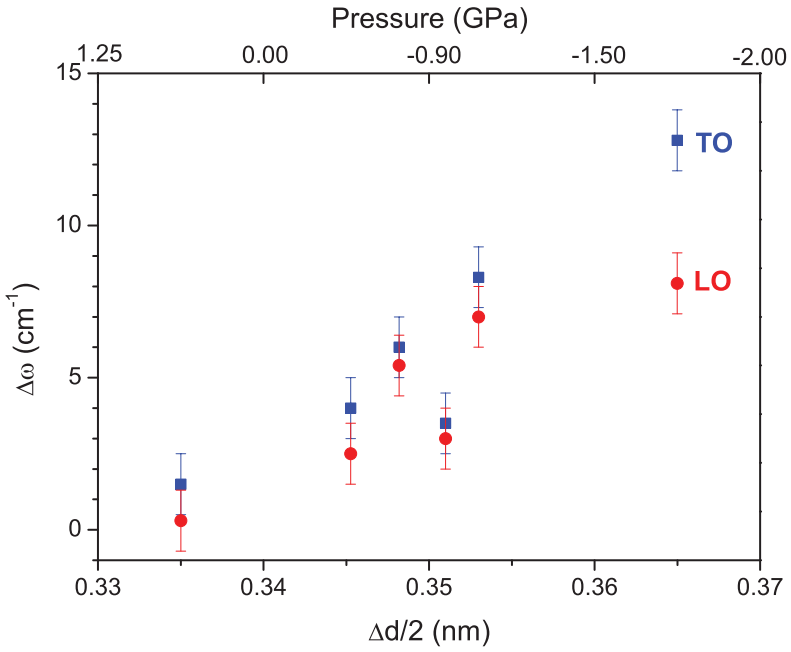

Figure 8: Dependence of the downshift of the LO (solid red dots) and TO (solid blue squares) G-modes of the inner layer with respect to the frequency of the corresponding G-modes in related SWNTs as a function of the inter-layer distance (bottom scale) and the deduced non linear pressure scale (top scale) following the procedure of Ref.[12] (see text).

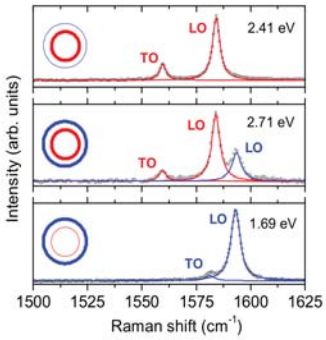

Graphic.jpg

Figure 9: TOC Graphic